



# The rupture risk of intracranial saccular aneurysm: a case—control study based on a three-dimensional computed tomography angiography model

Yueyun Chen<sup>#</sup>, Jiayang Wu<sup>#</sup>, Wenxia Yuan, Wenfeng Mai, Hengguo Li

Department of Medical Imaging, The First Affiliated Hospital of Jinan University, Jinan University, Guangzhou, China

*Contributions:* (I) Conception and design: Y Chen, H Li; (II) Administrative support: Y Chen, J Wu, W Yuan, W Mai; (III) Provision of study materials or patients: Y Chen, J Wu, W Mai; (IV) Collection and assembly of data: Y Chen, W Yuan; (V) Data analysis and interpretation: Y Chen, J Wu, W Mai; (VI) Manuscript writing: All authors; (VII) Final approval of manuscript: All authors.

<sup>#</sup>These authors contributed equally to this work.

*Correspondence to:* Hengguo Li, MD, PhD. Department of Medical Imaging, The First Affiliated Hospital of Jinan University, No. 601 Huangpu Avenue West, Tianhe District, Guangzhou 510630, China. Email: lhgju@263.net.

**Background:** Assessing the risk of rupture in intracranial aneurysms is crucial. Advancements in medical imaging now allow for three-dimensional (3D) assessments of aneurysms, providing a more detailed understanding of their morphology and associated risks. This study aimed to compare the 3D morphological parameters of ruptured and unruptured intracranial saccular aneurysms (ISAs) using computed tomography angiography (CTA) and to analyze risk factors linked to ISA rupture.

**Methods:** This retrospective case—control study included patients diagnosed with ISAs via CTA, for which data were sourced from both the Emergency Department and Inpatient Unit in The First Affiliated Hospital of Jinan University. The patients were categorized into rupture and unrupture groups. We used 3D-Slicer (version 5.2.2, Slicer Community) to construct morphological models of the ISAs and their parent arteries. These models facilitated assessments of intracranial aneurysmal volume (IAV), aneurysmal surface area (ASA), and maximum sectional area (MSA). Differences in 3D morphological parameters between ruptured and unruptured ISAs were then analyzed. For statistical analysis, we first performed single factor analysis on the data, constructed a receiver operating characteristic (ROC) curve one by one with statistically significant parameters, and screened out ROC curves that met the sample requirements. Second, we performed multiparameter logistic regression analysis to construct a ROC curve model and analyzed its predictive performance.

**Results:** The analysis encompassed 97 patients comprising 97 ISAs diagnosed from March 2016 to March 2022. Significant differences in morphological parameters were observed between the rupture and unrupture groups ( $P < 0.05$ ), including IAV, ASA, MSA, IAV/diameter (IAV/D), IAV/neck width (IAV/N), MSA/diameter (MSA/D), MSA/neck width (MSA/N), ASA/neck width (ASA/N), and ASA/MSA. It was found that the IAV, ASA, and MSA values of the rupture group were larger than those of the unrupture group. Meanwhile, the IAV/D, IAV/N, MSA/D, MSA/N, and ASA/N values were larger in the rupture group, while ASA/MSA and ASA/IAV were smaller.

**Conclusions:** This study underscores the significance of specific morphological indicators, such as ASA/N and ASA/MSA, in predicting the rupture risk of ISAs. The IAV, MSA, and ASA parameters, especially in relation to diameter and neck width, provide crucial insights into the rupture potential of ISAs.

**Keywords:** Intracranial saccular aneurysms (ISAs); computed tomography angiography (CTA); morphology

Submitted Nov 28, 2023. Accepted for publication Mar 04, 2024. Published online Apr 07, 2024.

doi: 10.21037/qims-23-1694

View this article at: <https://dx.doi.org/10.21037/qims-23-1694>

## Introduction

Intracranial aneurysms, marked by the pathological dilation of cerebral artery and its branches, account for about 80–85% of spontaneous subarachnoid hemorrhages (SAH) (1). SAH resulting from ruptured intracranial aneurysms is associated with a high mortality rate of about 35% (2). Recent advancements in medical imaging such as high-resolution magnetic resonance vessel wall imaging (HRMR VWI) and four-dimensional computed tomography angiography (4D-CTA), have led to a higher detection rate of cerebral aneurysms. However, HRMR VWI may prolong the time to treatment due to its longer associated acquisition time. Nonetheless, these novel techniques may eventually replace digital subtraction angiography (DSA) as a first-line modality for diagnostic workup of intracranial aneurysms but remain to be popularized. For now, three-dimensional CTA (3D-CTA) is still the mainstream method for the diagnosis of intracranial saccular aneurysms (ISAs). As imaging technology continues to evolve, more accurate prediction of ISA rupture stands to inform the clinical decision-making regarding the need for intervention (3).

In recent years, there has been an increase in research focusing on the clinical, imaging, and hemodynamic factors of intracranial aneurysms. Identified risk factors for cerebral aneurysm rupture include age, hypertension, smoking, family history of cerebrovascular disease, and aneurysm size and location (4,5). For example, intracranial aneurysms exceeding 7 mm in length in the anterior communicating artery are at a higher risk of rupture (3). In addition to size and location, hemodynamic factors play a critical role in rupture risk, as the aneurysm's ground base, the width of aneurysm neck, and border on the parental artery also influence hemodynamics. For wide-neck aneurysms, as per Qiu *et al.* (6), the increased aneurysm volume results in intensified eddy currents and wall shear stress, making them more susceptible to rupture (6). Moreover, the inflow angle of intracranial aneurysms affects blood flow patterns (7). Elevated inflow angles correlate with increased blood flow velocity and pressure at the aneurysm apex, heightening

rupture risk (8,9). As these angles enlarge, blood flow becomes more turbulent, accelerating aneurysm growth and leading to potential rupture (10).

In recent years, the staging scoring methods used to evaluate the risk of intracranial aneurysm rupture include the Population, Hypertension, Age, Size, Earlier Subarachnoid Hemorrhage, and Site (PHASES) score (11) and Earlier Subarachnoid Hemorrhage, Aneurysm Location, Age, Population, Aneurysm Size and Shape (ELAPSS) score (12). Predictive factors essentially include patient age, gender, hypertension, history of subarachnoid hemorrhage, geographic region, and aneurysm size and location. While current scoring methods for rupture prediction include various factors, they often lack the 3D morphological characteristics of ISAs. Due to the limited number of previous studies on 3D morphological features, there is currently a lack of systematic evidence demonstrating the impact of these features on aneurysm rupture. Previous research has predominantly focused on 2D morphological analysis of aneurysms, resulting in scoring systems that primarily only involve 2D morphological features. This study, therefore, aimed to identify the differences in 3D morphological features between ruptured and unruptured ISAs to better understand the risk factors for rupture. We present this article in accordance with the STROBE reporting checklist (available at <https://qims.amegroups.com/article/view/10.21037/qims-23-1694/rc>).

## Methods

### *Study population*

This retrospective case-control study comprised 97 patients who were diagnosed with ISAs in the Emergency Department and Inpatient Unit of The First Affiliated Hospital of Jinan University between March 2016 and March 2022. The inclusion criteria were as follows: (I) patients diagnosed with intracranial aneurysms via DSA CTA, (II) patients with ISAs, and (III) patients with complete medical imaging data. Meanwhile, the exclusion

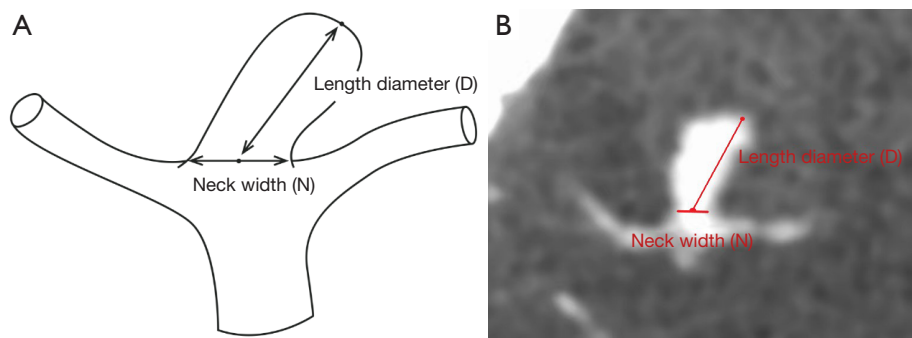


**Figure 1** Illustration and CTA image of ISA. (A) Illustration of the length diameter and neck width of ISA. (B) CTA image of the ISA with the length diameter and neck width. CTA, computed tomography angiography; ISA, intracranial saccular aneurysm.

criteria were as follows: (I) patients with fusiform, dissecting aneurysms, or pseudo-aneurysms diagnosed by any angiographic imaging method; (II) patients with aneurysms and comorbid moyamoya disease, cerebral arteriovenous malformations, or cerebral arteriovenous fistulas; (III) patients with recurrent aneurysms posttreatment; and (IV) patients with incomplete medical imaging data.

The rupture group included patients with aneurysmal subarachnoid hemorrhage confirmed by CTA or DSA, which often manifests clinically as headache, vomiting, nuchal rigidity, cranial nerve dysfunction, or altered consciousness (2). The unrupture group included patients with intracranial aneurysms identified during routine examinations or other diagnostic procedures who did not have a history of any type of SAH or a confirmed history of ruptured aneurysms (1). The study was conducted in accordance with the Declaration of Helsinki (as revised in 2013) and was approved by Institutional Review Board of The First Affiliated Hospital of Jinan University. The need for individual consent in this retrospective analysis was waived.

### *Image acquisition*

CTA of the skull was performed using a 320-slice CT scanner (Aquilion ONE, Toshiba Corporation, Japan). The scan covered a 16 cm range with a rotation time of 0.5 seconds. The reconstruction layer thickness was 0.5 mm, and the field of view (FOV) was 24 cm. The scanning tube voltage and current were set a 100 kV and 200 mA, respectively. A nonionic contrast agent, ioprotamine (concentration 350 mg I/mL; Bayer HealthCare Pharmaceuticals, Germany)

was administered intravenously at a volume of 60 mL and an injection flow rate of 4.0 mL/s. A bolus tracking technique synchronized the head CTA with a standard plain CT scan of the head. The region of interest was placed at the internal carotid artery's proximal segment, with image acquisition starting when the CT value reached 100 Hounsfield units (HU) within 3 seconds and lasted for 3–4 seconds.

### *Image processing and parameter calculation*

The 2D morphological features of ISAs, including diameter (D) and neck width (N), were repeatedly measured on the original CTA images (*Figure 1*) by two radiologists (radiologist A: Y.C.; radiologist B: W.M.). The two radiologists were provided the location of the aneurysms but were not aware of additional information. They conducted independent measurements, and in case of disagreement, they discussed the measurement until consensus was achieved. Radiologists A analyzed all ISAs, while radiologists B analyzed half of the ISAs provided randomly from each group. The 3D models of ISAs and their parental arteries were delineated using 3D Slicer software (version 5.2.2, Slicer Community) (13). The obtained subtraction CTA sequence was exported in DICOM format and copied to 3D-Slicer software for review. The main steps for image processing were as follows. (I) For CTA reconstruction, the threshold selection tool (*Threshold*) in the Segment Editor module was used to adjust the threshold range to make the blood vessels clearer and to obtain a reconstructed picture of the blood vessels of the head. (II) For aneurysm 3D model building, the draw tool was used to build a 3D model of the aneurysm and parent artery. (III) For aneurysmal surface

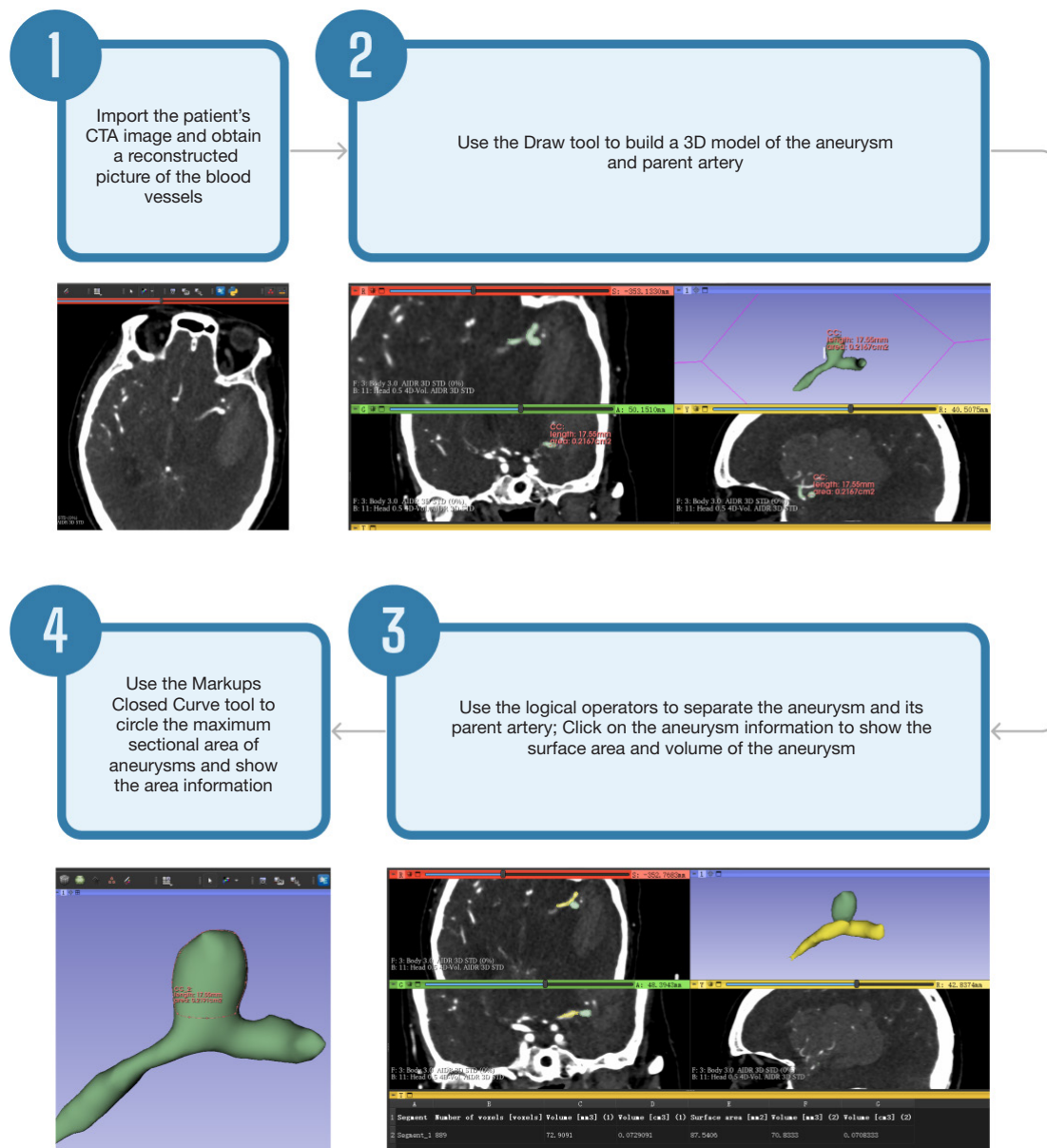


**Figure 2** The process of generating a 3D ISA model on 3D Slicer software. CTA, computed tomography angiography; 3D, three-dimensional; ISA, intracranial saccular aneurysm.

area (ASA) and volume measurement, a new segment was created with the Segment Editor module. A blank segmentation layer was created, and logical operators were used to perform addition (*Add*) and subtraction (*Subtract*) operations. Finally, two segmentation layers were obtained that were separate from the aneurysm and the parent artery. The surface area and volume of the aneurysm could be viewed by accessing the Models module. (IV) For aneurysm maximum sectional area (MSA) measurement method, the

Markups Closed Curve tool was used to circle the MSA of aneurysms. Area information was selected to display the MSA of aneurysms. Measurements were conducted twice, and the average was recorded (*Figure 2*).

The measurement indicators were defined as follows: D was the maximum distance from any point at the aneurysm's apex to the neck's midpoint, N was the longest diameter across the aneurysmal neck plane, intracranial aneurysmal volume (IAV) was the total volume occupied by the

aneurysm as assessed with 3D-Slicer, MSA was the largest projected area of the aneurysm as assessed with 3D-Slicer, and ASA was the aneurysm's outer surface area as assessed with 3D-Slicer.

The calculation indices were as follows: MSA/diameter (MSA/D), MSA/neck width (MSA/N), MSA/IAV, ASA/neck width (ASA/N), ASA/MSA, ASA/IAV, IAV/diameter (IAV/D), and IAV/neck width (IAV/N).

### Statistical methods

In this study, CTA was used to evaluate the sensitivity, specificity, accuracy, and the receiver operating characteristic (ROC) curve of 3D morphological features in predicting aneurysm rupture. SPSS version 26.0 (IBM Corp.) was used to analyze the research data. The normality of quantitative data was evaluated with the Shapiro-Wilk test. Quantitative data with a normal distribution are expressed as  $\bar{x} \pm s$ , and the paired sample *t*-test was used for comparison between groups. Meanwhile, quantitative data with a nonnormal distribution are expressed as median and interquartile range. The Wilcoxon rank sum test of paired samples was used for comparison between groups. Weighted kappa ( $\kappa$ ) statistics were used to assess interobserver agreement for the measurement. A weighted  $\kappa$  value >0.81 was considered excellent agreement, 0.61–0.80 good, 0.41–0.60 moderate, 0.21–0.40 poor, and <0.21 very poor. The enumeration data were analyzed with the  $\chi^2$  test, and the measurement data were analyzed with the *t*-test and rank sum test. The meaningful indicators were identified with the DeLong test (14) so that the ROC curves of the participants could be drawn. Because the sample size of this study was small, according to the condition of events per variable (EPV) required by multivariate logistic regression, the EPV was set to 10; that is, if the minimum number of events per independent variable *X* (the number of intracranial aneurysms in this study) were 10–11, then the number of morphological features included in the model would be 4 (15). The selection of 4 was based on the fact that the unrupture (smaller) group consisted of 44 participants, resulting in an average ratio of 4.4 (or 4) per feature. According to the area under the curve (AUC), 4–5 morphological features with better diagnostic efficacy were selected, and the logistic regression model was

established with the stepwise method. This model identified the independent risk factors, and an ROC curve was drawn for the predictive factors, and the AUC was calculated. There were no missing data in this study.

## Results

### General characteristics of the study population

We initially collected the CTA imaging data of 174 patients. After screening (*Figure 3*), there were 97 patients (40 males and 57 females; age  $61 \pm 11$  years), comprising 97 ISAs, who were divided into a rupture group ( $n=53$ ) and a unrupture group ( $n=44$ ). In the rupture group, DSA was performed in 21 cases, accounting for 40% of the total number of ruptured cases. Conversely, in the unrupture group, DSA was conducted in 30 cases, accounting for 68% of the total number of unruptured cases. After being diagnosed with intracranial aneurysm, 20 cases (38% of the rupture group) underwent clipping, 17 cases (32%) received embolization, and 16 cases (30%) did not undergo any operation. As for the unrupture group, 6 cases (14% of the unrupture group) underwent clipping, 7 cases (16%) received embolization, and 31 cases (70%) did not undergo any operation (*Table 1*).

### Interobserver agreement of the measurement indices

The interobserver agreement in all the measurement indices was excellent [IAV: weighted  $\kappa=0.816$ , 95% confidence interval (CI): 0.709–0.923; ASA: weighted  $\kappa=0.898$ , 95% CI: 0.813–0.982; MSA: weighted  $\kappa=0.877$ ; 95% CI: 0.785–0.969; D: weighted  $\kappa=0.816$ ; 95% CI: 0.708–0.923; N: weighted  $\kappa=0.855$ ; 95% CI: 0.757–0.953], as was the total agreement in all indices (weighted  $\kappa=0.852$ ; 95% CI: 0.754–0.950) (*Table 2*).

### Single factor analysis

This study incorporated three 3D morphological features: IAV, ASA, and MSA (*Table 3*). The Wilcoxon rank sum test for two independent samples revealed significant differences in IAV, ASA, and MSA between the ruptured and unruptured ISAs. The IAV in the rupture group was larger than that in the unrupture group ( $Z=-4.77$ ;  $P<0.05$ ), as was the ASA ( $Z=-4.44$ ;  $P<0.05$ ) and MSA ( $Z=-5.58$ ;  $P<0.05$ ).

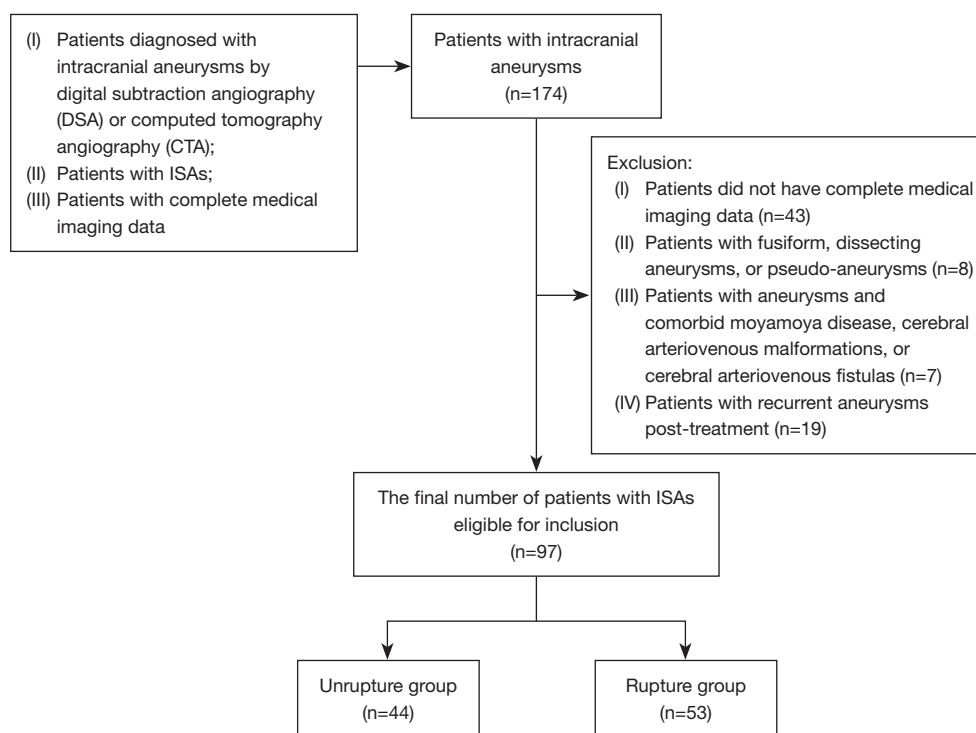


**Figure 3** Patient flow diagram. DSA, digital subtraction angiography; CTA, computed tomography angiography; ISA, intracranial saccular aneurysm.

**Table 1** General characteristics of the study population

Group	DSA completed	Procedure after diagnosis		
		Clipping	Embolization	Without operation
Rupture (n=53), n [%]	21 [40]	20 [38]	17 [32]	16 [30]
Unrupture (n=44), n [%]	30 [68]	6 [14]	7 [16]	31 [70]

DSA, digital subtraction angiography.

From these morphological measurements, additional features including IAV/D, IAV/N, MSA/D, MSA/N, MSA/IAV, ASA/D, ASA/N, ASA/MSA, and ASA/IAV were calculated (Table 3). Further Wilcoxon rank sum testing indicated significant differences in IAV/D, IAV/N, MSA/D, MSA/N, ASA/N, ASA/MSA, and ASA/IAV between the rupture and unrupture groups. The result showed that IAV/D ( $Z=-3.34$ ;  $P<0.05$ ), IAV/N ( $Z=-5.39$ ;  $P<0.05$ ), MSA/D ( $Z=-3.76$ ;  $P<0.05$ ), MSA/N ( $Z=-4.00$ ;  $P<0.05$ ), and ASA/N ( $Z=-6.12$ ;  $P<0.05$ ) were larger in the rupture group while ASA/MSA ( $Z=-4.85$ ;  $P<0.05$ ) and ASA/IAV ( $Z=-5.12$ ;  $P<0.05$ ) were smaller.

### ***Establishment and evaluation of the predictive model***

The ROC curve was plotted for the aforementioned 10 morphological features, and the AUC was calculated (Table 4). ASA/N and ASA/MSA were identified as having high predictive efficacy. The rupture of the aneurysm was considered to be the dependent variable (rupture =1, unrupture =0). After stepwise logistic regression was conducted, ASA/N and ASA/MSA emerged as independent predictors of aneurysm rupture (Table 3). The AUC for ASA/N was 0.862, with a sensitivity of 87% and a specificity of 66%. For ASA/MSA, the AUC was 0.873, with a sensitivity of 91% and a specificity of 57% (Table 5) (Figure 4).

The logistic regression equation was as follow:

$$P = eX / (1 + eX) \quad [1]$$

where *P* is the prediction probability, *e* is the natural logarithm, and *X* = 1.778 + (2.898 × ASA/N) – (1.876 × ASA/MSA). This model assessed the probability of aneurysm rupture, and its ROC curve was drawn. The resulting AUC was 0.938, with a sensitivity of 93.8% and a

**Table 2** Agreement of measurement indices between the two radiologists

Measurement index	Agreement, weighted κ	95% CI
IAV	0.816	0.709–0.923
ASA	0.898	0.813–0.982
MSA	0.877	0.785–0.969
D	0.816	0.708–0.923
N	0.855	0.757–0.953
Total	0.852	0.754–0.950

CI, confidence interval; IAV, intracranial aneurysm volume; ASA, aneurysmal surface area; MSA, maximum sectional area; D, intracranial aneurysm length diameter; N, intracranial aneurysmal neck width.

**Table 4** Rupture prediction efficacy for intracranial saccular aneurysms of 10 morphological parameters

Variable	SE	AUC (95% CI)
IAV	0.049	0.787 (0.692–0.882)
MSA	0.042	0.830 (0.747–0.913)
ASA	0.050	0.762 (0.664–0.860)
IAV/D	0.055	0.678 (0.571–0.786)
IAV/N	0.044	0.821 (0.736–0.907)
MSA/D	0.052	0.724 (0.622–0.825)
MSA/N	0.034	0.782 (0.806–0.941)
ASA/N	0.036	0.862 (0.791–0.933)
ASA/MSA	0.047	0.873 (0.694–0.879)
ASA/IAV	0.045	0.816 (0.727–0.904)

SE, standard error; AUC, area under the curve; CI, confidence interval; IAV, intracranial aneurysmal volume; MSA, maximum sectional area; ASA, aneurysmal surface area; IAV/D, intracranial aneurysmal volume/length diameter; IAV/N, intracranial aneurysmal volume/neck width; MSA/D, maximum sectional area/length diameter; MSA/N, maximum sectional area/neck width; ASA/N, aneurysmal surface area/neck width; ASA/MSA, aneurysmal surface area/maximum sectional area; ASA/IAV, aneurysmal surface area/intracranial aneurysm volume.

**Table 3** Comparison of 3D morphological parameters between the intracranial saccular rupture group and the unrupture group

Morphological parameter	Rupture group (n=53)	Unrupture group (n=44)	Z	P
IAV	0.09 (0.06, 0.19)	0.04 (0.03, 0.07)	–4.77	<0.05
MSA	0.28 (0.20, 0.48)	0.14 (0.09, 0.19)	–5.58	<0.05
ASA	1.04 (0.80, 1.78)	0.57 (0.47, 0.91)	–4.44	<0.05
IAV/D	0.15 (0.11, 0.26)	0.11 (0.08, 0.17)	–3.34	<0.05
IAV/N	0.27 (0.19, 0.58)	0.13 (0.09, 0.20)	–5.39	<0.05
MSA/D	0.43 (0.38, 0.56)	0.36 (0.30, 0.42)	–3.76	<0.05
MSA/N	0.62 (0.49, 0.82)	0.35 (0.28, 0.47)	–4.00	<0.05
ASA/N	3.22 (2.39, 5.46)	1.78 (1.53, 2.43)	–6.12	<0.05
ASA/MSA	4.04 (3.55, 4.86)	5.31 (4.36, 6.22)	–4.85	<0.05
ASA/IAV	11.50 (9.10, 13.50)	16.41 (13.14, 17.93)	–5.12	<0.05
MSA/IAV	2.73 (2.23, 3.42)	2.97 (2.21, 3.73)	–0.96	>0.05
ASA/D	1.71 (1.44, 2.47)	1.71 (1.49, 2.36)	–0.24	>0.05

Data are presented as median (first quartile, third quartile). 3D, three-dimensional; IAV, intracranial aneurysmal volume; MSA, maximum sectional area; ASA, aneurysmal surface area; IAV/D, intracranial aneurysmal volume/length diameter; IAV/N, intracranial aneurysmal volume/neck width; MSA/D, maximum sectional area/length diameter; MSA/N, maximum sectional area/neck width; ASA/N, aneurysmal surface area/neck width; ASA/MSA, aneurysmal surface area/maximum sectional area; ASA/IAV, aneurysmal surface area/intracranial aneurysm volume; MSA/IAV, maximum sectional area/intracranial aneurysmal volume; ASA/D, aneurysmal surface area/length diameter.

**Table 5** Estimates of independent variables and related parameters included in the logistic regression equation

Variable	Coefficient	P	OR (95% CI)	Sensitivity (95% CI)	Specificity (95% CI)
ASA/N	2.898	0.01	18.146 (3.966–83.019)	87% (0.827–0.979)	66% (0.614–0.914)
ASA/MSA	−1.876	0.01	0.153 (0.059–0.399)	91% (0.900–1.000)	57% (0.433–0.742)
Constant	1.778	0.027	–	–	–

OR, odds ratio; CI, confidence interval; ASA/N, aneurysmal surface area/neck width; ASA/MSA, aneurysmal surface area/maximum sectional area.

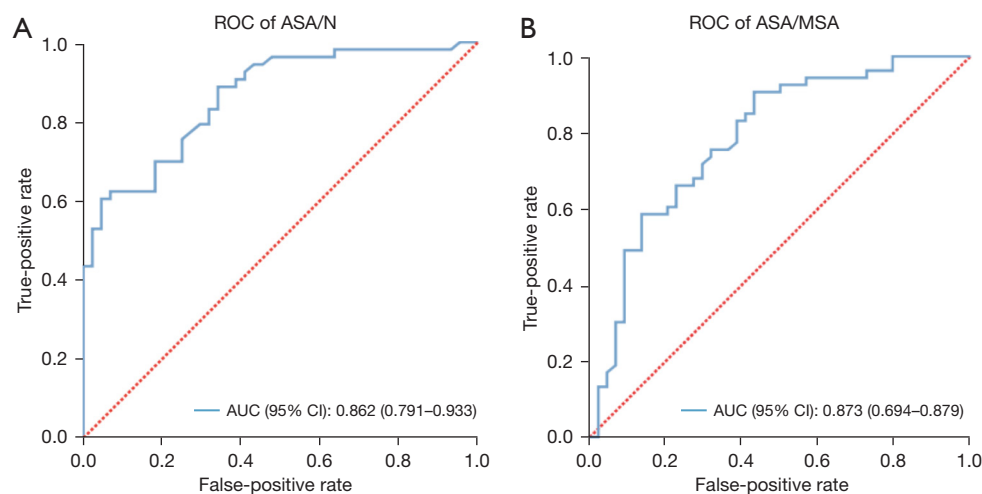


**Figure 4** The ROC of ASA/N and ASA/MSA. (A) The ROC of ASA/N. (B) The ROC of ASA/MSA. ROC, receiver operating characteristic; ASA/N, aneurysmal surface area/neck width; ASA/MSA, aneurysmal surface area/maximum sectional area; AUC, area under the curve; CI, confidence interval.

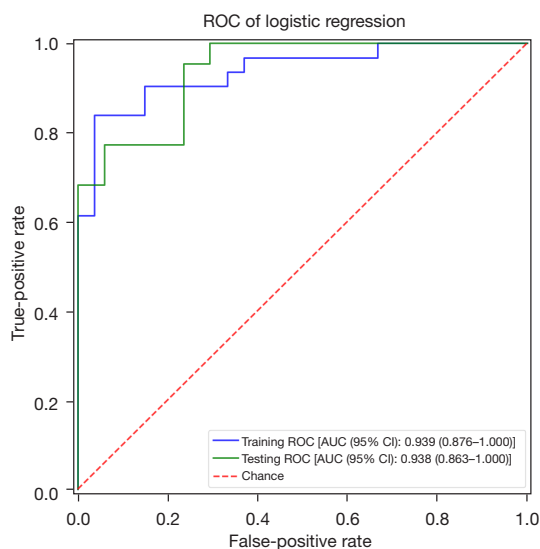


**Figure 5** The ROC of the combined model. ROC, receiver operating characteristic curve; AUC, area under the curve; CI, confidence interval.

specificity of 58.82% (Figure 5).

## Discussion

In this study, we observed that the rupture group exhibited significantly larger IAV, ASA, and MSA values compared to the unrupture group. Additionally, the IAV/D, IAV/N, MSA/D, MSA/N, and ASA/N values were higher in the rupture group while the ASA/MSA and ASA/IAV values were lower.

We conducted a comprehensive analysis of the imaging characteristics exhibited by 53 cases of ruptured ISAs and 44 cases of unruptured ISAs. A 3D model of ISAs and their parent arteries was constructed using 3D-Slicer. Two independent researchers measured the 3D morphological features of each aneurysm, including ASA, IAV, and MSA. Aneurysm body diameter and neck width were measured on multiplanar CTA images. This method enhanced the accuracy of calculating 3D measurement parameters, as



the dimensions of the aneurysm body and neck width are directly linked to the risk of rupture. Given the prevalence of ISAs in clinical settings, this study focused solely on ISAs. The findings indicated that the IAV, ASA, and MSA values were higher in the rupture group than in the unrupture group. Research by Villablanca *et al.* (16) also indicated there to be a correlation between aneurysm rupture and volume expansion rate. The risk of rupture escalates with volume expansion, leading to a greater likelihood of vortex formation, erratic intra-aneurysmal blood flow, and abnormal pulsation points on the aneurysm wall. The degree of these abnormal pulsations reflects the structural weakness of the wall (17), with more pulsations indicating a more fragile wall structure and thus an increased risk of rupture. As aneurysms expand, their ASA increases due to the stretching of the aneurysm surface. Histological examination reveals that aneurysm walls often have only an intima, lacking medial smooth muscle tissue and elastic fibers or exhibiting breaks in elastic fibers, reducing wall compliance (18). With the analogy of an aneurysm as a balloon, blood flow is akin to gas entering the balloon: the more the gas fills the balloon, the faster the volume and ASA increase. A thinner balloon wall implies greater instability and a higher likelihood of rupture. Therefore, the ASA of an aneurysm partly reflects the wall's structural weakness, with a larger ASA indicating a higher likelihood of rupture. Additionally, the MSA of an aneurysm, representing its maximum projected area, signifies the aneurysm's size. A larger MSA suggests a larger aneurysm length and diameter, correlating with an increased risk of rupture.

Given the complexity of the rupture mechanism in intracranial aneurysms, relying solely on one factor for rupture prediction is insufficiently representative. Hence, we included additional calculated parameters in our measurement index, including IAV/D, IAV/N, MSA/D, MSA/N, MSA/IAV, ASA/D, ASA/N, ASA/MSA, and ASA/IAV. In the rupture group, the IAV/D, IAV/N, MSA/D, MSA/N, and ASA/N values were larger, while the ASA/MSA and ASA/IAV values were lower. Multivariate logistic regression analysis indicated that ASA/N and ASA/MSA were independent risk factors for aneurysm rupture. Larger ASA/N values suggest a larger ASA, weaker aneurysm wall stability, and a narrower neck. Previous studies have demonstrated that blood flow velocity within the aneurysm decreases as the neck narrows and the volume increases. Geometric features that signal an increased risk of rupture, such as variations in balloon and aneurysm size, are closely linked to low flow velocities. In aneurysms with low flow,

high aneurysmal pressure and intra-aneurysmal blood pooling are key contributors to rupture. Elevated ASA/N values further encourage blood pooling within the aneurysm, leading to vessel wall changes that precipitate rupture (19). Blood flow within an aneurysm is partly determined by the product of blood flow velocity and the aneurysm's cross-sectional area. As the aneurysm's maximum cross-sectional area increases, more blood enters the aneurysm, raising the risk of intra-aneurysmal accumulation and potential vessel wall damage. This underscores that lower ASA/MSA values not only increase blood flow within the aneurysm but also contribute to increased aneurysm volume and enlarged ASA, aggravating the instability of ISAs and ultimately leading to rupture.

Some limitations to this study should be mentioned. First, this study employed a relatively small sample size and a retrospective, single-center design. These factors may limit the generalizability of our findings in the broader population. Future studies should be larger and multicentered to validate and enhance the robustness of these findings. Second, it is important to acknowledge that the use of a hand-drawn model in 3D Slicer might have introduced some bias, possibly affecting the evaluation to a certain degree.

## Conclusions

In this study, the ASA/N and ASA/MSA values served as independent risk factors for predicting ruptured ISAs. The results of this study contribute to a deeper understanding of the diverse morphological characteristics associated with ruptured intracranial aneurysms and offer valuable insights for both pre- and postoperative management.

## Acknowledgments

We would like to thank all members of Jinan University for helpful discussions.

*Funding:* None.

## Footnote

*Reporting Checklist:* The authors have completed the STROBE reporting checklist. Available at <https://qims.amegroups.com/article/view/10.21037/qims-23-1694/rc>

*Conflicts of Interest:* All authors have completed the ICMJE uniform disclosure form (available at <https://qims.amegroups.com/article/view/10.21037/qims-23-1694/rc>)

[amegroups.com/article/view/10.21037/qims-23-1694/coif](https://amegroups.com/article/view/10.21037/qims-23-1694/coif)). The authors have no conflicts of interest to declare.

**Ethical Statement:** The authors are accountable for all aspects of the work in ensuring that questions related to the accuracy or integrity of any part of the work are appropriately investigated and resolved. This study was conducted in accordance with the Declaration of Helsinki (as revised in 2013) and was approved by the Institutional Review Board of The First Affiliated Hospital of Jinan University. The need for individual consent in this retrospective analysis was waived.

**Open Access Statement:** This is an Open Access article distributed in accordance with the Creative Commons Attribution-NonCommercial-NoDerivs 4.0 International License (CC BY-NC-ND 4.0), which permits the non-commercial replication and distribution of the article with the strict proviso that no changes or edits are made and the original work is properly cited (including links to both the formal publication through the relevant DOI and the license). See: <https://creativecommons.org/licenses/by-nc-nd/4.0/>.

## References

- Brown RD Jr, Broderick JP. Unruptured intracranial aneurysms: epidemiology, natural history, management options, and familial screening. *Lancet Neurol* 2014;13:393-404.
- Nieuwkamp DJ, Setz LE, Algra A, Linn FH, de Rooij NK, Rinkel GJ. Changes in case fatality of aneurysmal subarachnoid haemorrhage over time, according to age, sex, and region: a meta-analysis. *Lancet Neurol* 2009;8:635-42.
- Etminan N, Rinkel GJ. Unruptured intracranial aneurysms: development, rupture and preventive management. *Nat Rev Neurol* 2016;12:699-713.
- Juvela S, Porras M, Poussa K. Natural history of unruptured intracranial aneurysms: probability and risk factors for aneurysm rupture. *Neurosurg Focus* 2000;8:Preview 1.
- Juvela S, Poussa K, Lehto H, Porras M. Natural history of unruptured intracranial aneurysms: a long-term follow-up study. *Stroke* 2013;44:2414-21.
- Qiu T, Jin G, Xing H, Lu H. Association between hemodynamics, morphology, and rupture risk of intracranial aneurysms: a computational fluid modeling study. *Neurol Sci* 2017;38:1009-18.
- Liou TM, Li YC, Juan WC. Numerical and experimental studies on pulsatile flow in aneurysms arising laterally from a curved parent vessel at various angles. *J Biomech* 2007;40:1268-75.
- Baharoglu MI, Schirmer CM, Hoit DA, Gao BL, Malek AM. Aneurysm inflow-angle as a discriminant for rupture in sidewall cerebral aneurysms: morphometric and computational fluid dynamic analysis. *Stroke* 2010;41:1423-30.
- Fan J, Wang Y, Liu J, Jing L, Wang C, Li C, Yang X, Zhang Y. Morphological-Hemodynamic Characteristics of Intracranial Bifurcation Mirror Aneurysms. *World Neurosurg* 2015;84:114-120.e2.
- Meng H, Metaxa E, Gao L, Liaw N, Natarajan SK, Swartz DD, Siddiqui AH, Kolega J, Mocco J. Progressive aneurysm development following hemodynamic insult. *J Neurosurg* 2011;114:1095-103.
- Greving JP, Wermer MJ, Brown RD Jr, Morita A, Juvela S, Yonekura M, Ishibashi T, Torner JC, Nakayama T, Rinkel GJ, Algra A. Development of the PHASES score for prediction of risk of rupture of intracranial aneurysms: a pooled analysis of six prospective cohort studies. *Lancet Neurol* 2014;13:59-66.
- Wiley JZ. Reader response: ELAPSS score for prediction of risk of growth of unruptured intracranial aneurysms. *Neurology* 2018;90:1038-9.
- Cheng GZ, San Jose Estepar R, Folch E, Onieva J, Gangadharan S, Majid A. Three-dimensional Printing and 3D Slicer: Powerful Tools in Understanding and Treating Structural Lung Disease. *Chest* 2016;149:1136-42.
- DeLong ER, DeLong DM, Clarke-Pearson DL. Comparing the areas under two or more correlated receiver operating characteristic curves: a nonparametric approach. *Biometrics* 1988;44:837-45.
- Peduzzi P, Concato J, Kemper E, Holford TR, Feinstein AR. A simulation study of the number of events per variable in logistic regression analysis. *J Clin Epidemiol* 1996;49:1373-9.
- Villablanca JP, Duckwiler GR, Jahan R, Tateshima S, Martin NA, Frazee J, Gonzalez NR, Sayre J, Vinuela FV. Natural history of asymptomatic unruptured cerebral aneurysms evaluated at CT angiography: growth and rupture incidence and correlation with epidemiologic risk factors. *Radiology* 2013;269:258-65.
- Zhang J, Li X, Zhao B, Zhang J, Sun B, Wang L, Tian J, Mossa-Basha M, Kim LJ, Yan J, Wan J, Xu J, Zhou Y, Zhao H, Zhu C. Irregular pulsation of aneurysmal wall is associated with symptomatic and ruptured intracranial

- aneurysms. *J Neurointerv Surg* 2023;15:91-6.
18. Xu Z, Rui YN, Hagan JP, Kim DH. Intracranial Aneurysms: Pathology, Genetics, and Molecular Mechanisms. *Neuromolecular Med* 2019;21:325-43.
  19. Ujiie H, Tamano Y, Sasaki K, Hori T. Is the aspect ratio a reliable index for predicting the rupture of a saccular aneurysm? *Neurosurgery* 2001;48:495-502; discussion 502-3.

**Cite this article as:** Chen Y, Wu J, Yuan W, Mai W, Li H. The rupture risk of intracranial saccular aneurysm: a case—control study based on a three-dimensional computed tomography angiography model. *Quant Imaging Med Surg* 2024;14(5):3339-3349. doi: 10.21037/qims-23-1694